Behaviour of palladium in three lateritic profiles developed on serpentinites of the Lomié ultramafic complex, South-East Cameroon

NDJIGUI Paul-Désiré
Department of Earth Sciences, University of Yaoundé I, P. O. Box: 812 Yaoundé - Cameroon

ABSTRACT

Palladium is one of the platinum-group elements (PGE); its research is very important considering the price on the world market. In the weathered profiles developed on serpentinites in the Lomié region (South-East Cameroon), slightly elevated Pd contents are observed in the coarse saprolite (28-40 ppb), in the nodules (20-22 ppb) and in the pisolitic iron duricrust (38 ppb). Apart from these hardened materials (nodules, pisolitic iron duricrust), the Pd contents decrease upwards in the weathering profile. The high Pd contents in the coarse saprolite are due to the supergene enrichment and secondary Pd precipitation processes. In the hardened materials, they are instead as result their ferruginous and very hardened nature that offer resistance to the leaching process activated by water charged with organic matter and carbon dioxide. Pd behaviour versus three most abundant major elements in the laterites (Fe, Si, Al) differs from one weathering profile to another.

Key words: Palladium - Cameroon - Serpentinites - Weathering - Laterites - Saprolite.

RÉSUMÉ

Le palladium constitue l'un des éléments du groupe du platine, ce sont des éléments qui possèdent une forte valeur marchande dont l'exploration est basée uniquement sur les critères géochimiques. Dans trois profils latéritiques développés sur serpentinites dans le complexe ultrabasique de Lomié (Sud-Est Cameroun), les teneurs élevées en palladium ont été observées dans la saprolite grossière (28-40 ppb), dans les nodules (20-22 ppb) et dans la cuirasse pisolitique (38 ppb). Hormis les matériaux fortement indurés (nodules et blocs de cuirasse pisolitique), les concentrations en palladium diminuent de la base vers le sommet des profils d'altération. La concentration élevée dans la saprolite grossière résulte d'un enrichissement supergène ou des processus de précipitation secondaire du palladium. Dans les matériaux ferrugineux fortement indurés, les teneurs élevées sont liées à la forte induration des matériaux qui leur offrent une certaine résistance vis-à-vis du lessivage des matériaux activé par les eaux chargées de gaz carbonique et de la matière organique. Les diagrammes binaires, établis entre le palladium et les trois éléments chimiques les plus abondants dans les latérites (Fe, Al, Si), montrent que les affinités entre ces éléments diffèrent d'un profil à un autre.

Mots clés: Palladium - Cameroun - Serpentinites - Altération - Latérites - Saprolite.

Corresponding author: NDJIGUI Paul-Désiré, Department of Earth Sciences, University of Yaoundé I, P.O. Box: 812 Yaoundé-Cameroon. E-mail: lndjigui@yahoo.fr

1. INTRODUCTION

The PGE constitute a group of six elements (Pt, Pd, Ir, Rh, Ru, Os) that are generally weakly represented in rocks, with concentrations globally lower than 10 ppb (Luguet et al. 2007; Godel et al. 2007; Godel and Barnes 2007). However, they are highly sought elements, because of their high metallogenic value. Among the PGE, platinum and palladium are used in many domains such as in automobile industry, electronics, jewellery .... Although of great economic importance, research on these elements has received less attention, probably due to the very high cost of analyses. Pt and Pd behaviour in the laterites developed on ultramafic rocks have been studied in the tropical region (Bowles 1986; Augé et al. 1995; Salpéteur et al. 1995; Ndjigui et al. 2003; Ndjigui et al. 2004; Traoré, 2005; Traoré et al. 2006). The aim of this work has been to study the behaviour of palladium in three lateritic profiles and to explain the mechanisms that could be controlling variations in Pd contents along each profile.

2. Geographical and geological setting

The Lomié ultramafic complex is situated in the South-East of Cameroon, within South Cameroon plateau (Fig. 1). This complex is made up of five bodies (Kongo-Nkamouna, Mang North, Mang

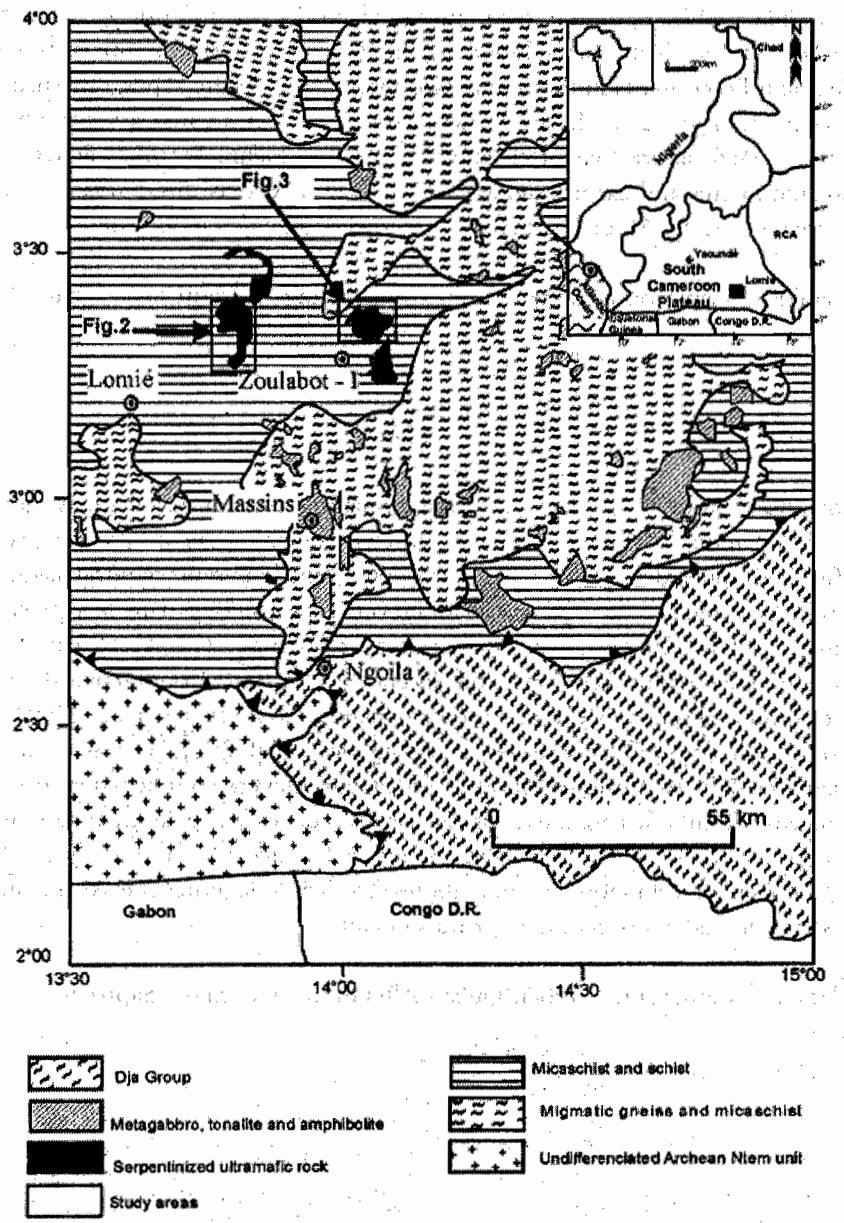

Figure 1: Geological map of the Lomié region (from Seme Mouangue 1998; modified by Toteu et al. 2006).

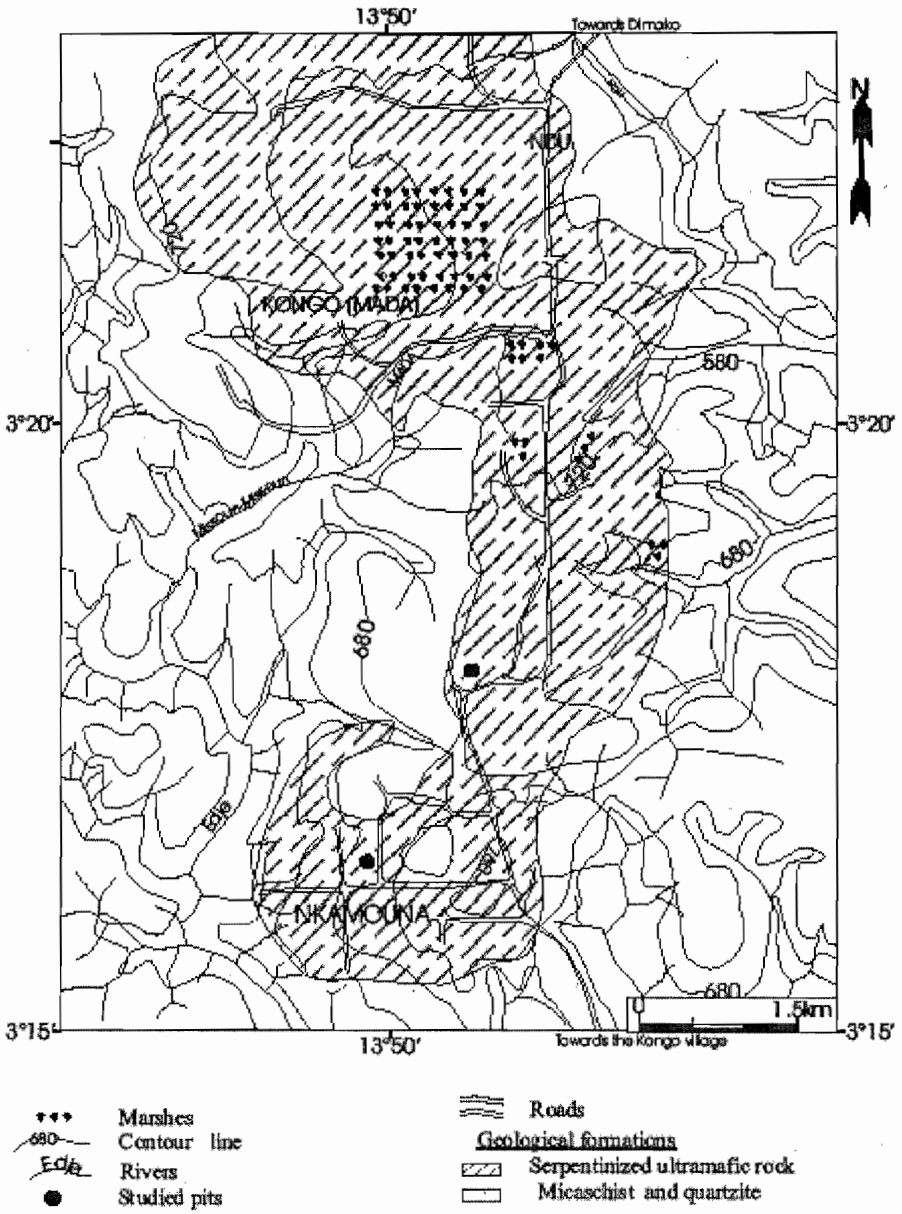

Figure 2: Sketch of geological and topographic map of Kongo-Nkamouna area and location of the studied pits.

South, Messea, Kondong I) with a surface area of about 240 km^2 (Fig. 1). The climate of the region is the guinean type characterized by four seasons (two rainy seasons and two dry seasons). The mean rainfall is 1655 mm/year and average temperature is 23.5°C (Suchel 1987). The vegetation is a dense rainforest (Letouzey 1985). The soils are red ferrallitic on hills and peneplains, and hydromorphic in the swampy depressions (Yongué-Fouateu 1995). The Lomié ultramafic complex is made up of serpentinites which are intruded by mica schists and schists (Seme Mouangué 1998) (Fig. 1). The country-rocks date from the Panafrican orogeny (Lasserre and Soba 1976; Toteu et al. 2006).

3. Analytical methods

Three weathering profiles were chosen to study the Pd behaviour in the lateritic profiles on the serpentinized ultramafic rocks of the Lomié complex. The Nkamouna and Napene weathering profiles are situated in the Kongo-Nkamouna body (Fig. 2) and that of Mang North is located in the body that carries the same name (Fig. 3). The samples collected were described and submitted to analyses in the Geoscience Laboratories of

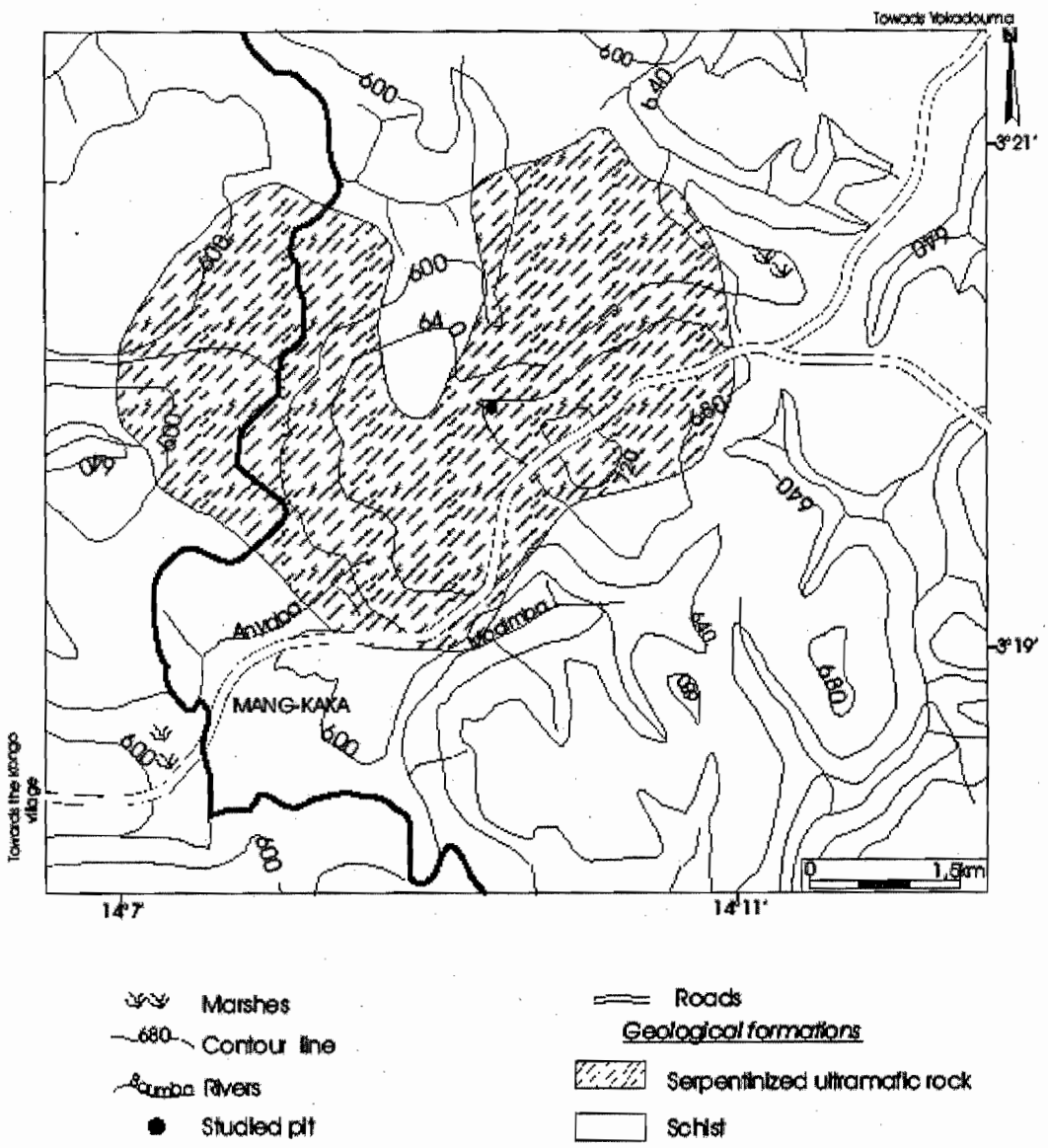

Figure 3: Sketch of geological and topographic map of Mang North area and location of the studied pit.

Ontario Geological Survey, Sudbury (Canada). The mineralogical analyses were carried out by X-ray diffraction analysis (XRD). The resulting diffraction spectra were compared with a computerized database of common minerals, whose automatic mineral-matching function was assisted by operator identification of phases consistent with the known compositions of the materials. Major element concentrations were determined by X-ray fluorescence (XRF) after sample ignition. Sample powders were ignited and then melted with a lithium tetraborate flux before analysis using a Rigaku RIX-3000 wavelength-dispersive X-ray fluorescence spectrometer.

The palladium data of twenty samples were produced by the Geoscience Laboratories of the Ontario Geological Survey in Sudbury (Canada) for the soil samples from the Nkamouna and Mang North lateritic profiles, and by Genalysis Laboratories Services (Australia) for the soil samples from Napene. Palladium was determined by a NiS fire assay with ICP-MS using a Perkin Elmer ELAN 500 instrument (Richardson and Burnham 2002).

Soil samples were mounted in epoxy and examined optically and also using an electron microscope to examine textures and perform qualitative

Table 1: Mineralogical composition of the parent rock and the weathered materials at Nkamouna.

Materials	Minerals					
	Antigorite	Quartz	Magnetite	Hematite	Goethite	Kaolinite
Loose clayey horizon	-	+	+	+++	-	++
Upper nodular horizon (nodules)	-	+	-	-	++	+
Upper nodular horizon (matrix)	-	+	+	-	+++	++
Lower nodular horizon (nodules)	-	+	+	-	+++	++
Lower nodular horizon (matrix)	-	+	+	-	+++	++
Fine saprolite	-	+	+	-	+++	++
Coarse saprolite (top)	-	-	++	-	+++	-
Coarse saprolite (bottom)	-	ε	+	-	+++	ε
Parent rock	+++	-	++	-	-	-

+++: very abundant; ++: abundant; +: poorly represented; ε : trace; -: absent.

energy-dispersive X-ray (EDS) analysis of selected mineral grains.

4. RESULTS

4.1. Petrology of serpentinites

The serpentinites are constituted by 90 % serpentine (antigorite), associated to opaque minerals (Tables 1, 3 and 5). The SiO_2 and MgO contents are high (36.67-38.99 wt.% SiO_2 and 38.20-39.70 wt.% MgO, respectively). Those of Fe_2O_3 (6.66-7.34 wt.%) and especially Al_2O_3 (1.00-2.27 wt.%) are much lower. Other major elements show either very low contents, less than 1 % for CaO (0.66 wt.%) or are less than the detection limit (Tables 2, 4 and 6). The Pd contents are very low in serpentinites (1.97 ppb in Nkamouna sample, <2 ppb in Napene sample, and 0.27 ppb in the Mang sample).

4.2. Description of weathering profiles, mineralogy and geochemistry of major elements

Table 2: Chemical composition [major elements (in wt %), Pd (in ppb)] of the parent rock and the weathered materials at Nkamouna.

		Parent rock	Coarse saprolite		Fine saprolite	Lower nodular horizon		Upper nodular horizon		Loose clayey horizon
			base	top		matrix	nodules	matrix	nodules	
Symbols		NK6	NK3	NK9	NK1	NK5	NK2	NK7	NK4	NK8
Depth(m)	-	-	18.00	11.50	9.00	5.60	5.60	1.50	1.50	0.50
	D.l.									
SiO_2	0.01	39.67	6.67	3.04	11.25	14.10	14.10	12.57	20.34	13.20
Al_2O_3	0.01	1.42	5.45	3.13	12.08	16.11	14.39	18.12	24.22	17.66
Fe_2O_3	0.01	6.66	82.07	89.04	62.11	53.99	56.63	51.05	38.08	50.59
MnO	0.01	0.06	1.24	0.47	2.06	0.50	0.57	0.42	0.06	0.48
MgO	0.01	39.66	0.80	0.45	0.60	0.33	0.32	0.32	0.06	0.32
CaO	0.01	< 0.01	< 0.01	< 0.01	< 0.01	< 0.01	< 0.01	< 0.01	< 0.01	< 0.01
Na_2O	0.01	0.02	0.02	< 0.01	0.02	0.02	0.01	0.02	< 0.01	0.01
K_2O	0.01	< 0.01	< 0.01	< 0.01	< 0.01	0.02	< 0.01	0.03	0.02	0.03
TiO_2	0.01	0.01	0.08	0.08	0.41	1.05	0.31	1.41	1.14	1.38
P_2O_5	0.01	< 0.01	< 0.01	< 0.01	0.04	0.07	0.03	0.10	0.06	0.11
LOI	0.05	11.80	6.29	6.68	8.81	10.81	10.20	12.44	13.38	12.49
Sum	-	99.30	102.62	102.89	97.38	97.00	96.56	96.748	94.36	96.27
Pd	0.11	1.97	15	12	13	13	20	11	22	10

D.l.: Detection limit.

4.2.1. Nkamouna weathering profile

The profile is located in the southern part of the ultramafic body (Fig. 2). This is 18.70 m deep above the water table and is made up, from the bottom to the top, of: a coarse saprolite, a fine saprolite, a lower nodular horizon, an upper nodular horizon and a loose clayey horizon (Fig. 4).

The coarse saprolite (8.7 m) is loose, with a sandy-silty texture and it is made up of a succession of horizontal millimetric layers showing a microbedded structure. The basal part of the coarse saprolite is goethitic. Accessory magnetite and kaolinite are represented (Table 1). The geochemical analyses of unweathered serpentinite (NK6) indicate 39.67 wt.% SiO_2, 39.66 wt.% MgO and 6.66 wt.% Fe_2O_3. SiO_2 decreases to 6.67% in the coarse saprolite and MgO 0.80%. Fe_2O_3 contents increase from 6.66 to 82.07 wt.% (Table 2). Aluminium contents change from parent serpentinite and coarse saprolite (5.45% Al_2O_3) whereas Mn contents increase from 0.06 to 1.24% (Table 2).

The uppermost part of this saprolite is made up mainly of goethite and magnetite (Table 1, Fig. 5). Fe_2O_3 contents increase to 89%, whereas SiO_2, Al2O3, MgO and MnO contents decrease (Table 2).

The coarse saprolite progressively transforms to the fine saprolite (2 m) in which the texture and the structure of the parent rock are still preserved. It shows numerous centimetric patches which are grey, loose, with a pasty texture and a microbedded structure. The silicates are completely weathered to goethite and kaolinite (Table 1) with accessory magnetite. The geochemical analyses (Table 2) indicate 11.25% SiO_2, 12.08% Al_2O_3, 62.11% Fe_2O_3 and 2.06% MnO. Accessory, it is composed of 0.6% MgO and 0.41% TiO_2 (Table 2).

Towards the top of the profile, the fine saprolite transforms to the nodular materials with a non-conservation of original structures. The first nodular material is the lower nodular horizon (3 m) which is made up of nodules embedded in a matrix.

The matrix is reddish, polyhedral, loose and porous. It has the same mineral assemblage as the fine saprolite (Table 1). The geochemical analyses indicate an increase in SiO_2 and Al_2O_3 (14.10% SiO_2 and 16.11% $Al2O_3$). Fe_2O_3 contents decrease to 53.99% (Table 2). Accessorily, this horizon is composed of 0.5% MnO, 0.33% MgO and 1.05% TiO_2 (Table 2).

The nodules (~70 % of soil) are centimetric, reddish brown, hardened, and spherical to sub-spherical. The mineral assemblage is dominated by goethite and kaolinite, with quartz and magnetite traces (Table 1). The geochemical analyses indicate an increase in Fe_2O_3 contents

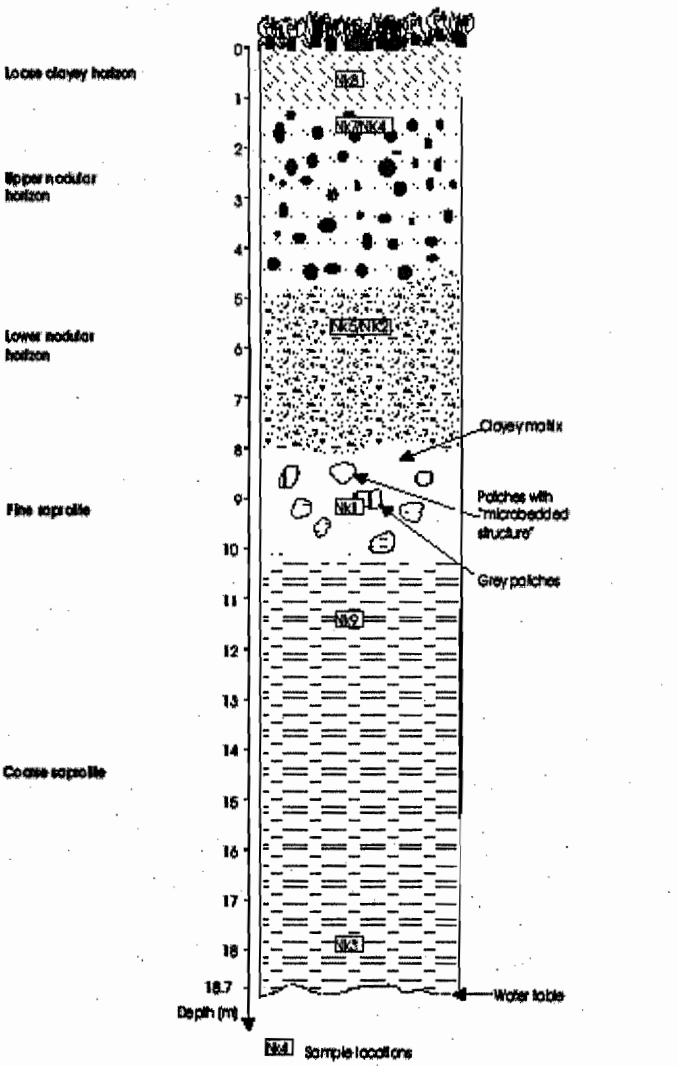

Figure 4: Description of Nkamouna weathering profile.

(56.63%) and a decrease in Al_2O_3 contents (14.39%).

The upper nodular horizon (4 m) is the second nodular material. It is constitutes by nodules that are embedded in the matrix. The matrix (~20 % of soil) has the same morphological organization and mineralogical composition as the matrix of the last nodular horizon (Table 1). The geochemical analyses reveal an increase in Al_2O_3 contents (18.12%), and a decrease in SiO_2 and Fe_2O_3 contents (51.05% Fe_2O_3 and 12.57% SiO_2). Accessorily, the matrix is composed of 0.42% MnO, 0.32% MgO, 1.41% TiO_2 and 0.1% P_2O_5 (Table 2).

The nodules (~80 % of soil) are very hard and present four to five concentric and reddish brown lobes that are held by a red ferruginous cement. The multilobed nodules are goethitic and slightly kaolinitic, with quartz traces (Table 1, Fig. 7). Fe_2O_3 contents decrease (38.08%); meanwhile, SiO_2, Al_2O_3 and TiO_2 contents show an opposite trend (20.34% SiO_2, 24.22% Al_2O_3 and 1.14% TiO_2) (Table 2).

The nodular material is overlained by a loose clayey horizon (1 m) which is friable, polyhedral, dark red, and porous. The mineral assemblage is dominated by hematite, kaolinite, quartz, with magnetite traces (Table 1). The geochemical analyses indicate an increase in Fe_2O_3 contents (50.59%) and the decrease of SiO_2 and Al_2O_3 contents (13.2% SiO_2 and 17.66% Al_2O_3).

4.2.2. Napene weathering profile

The Napene weathering profile is located to the North of Nkamouna (Fig. 2). Above the water table, the thickness of the weathering profile is up to 13.70 m and can be divided into four main layers from the bottom to the top: fine saprolite, nodular horizon, pisolitic iron duricrust and loose clayey horizon (Fig. 7).

The fine saprolite (3.70 m) is predominantly grey, sandy to clayey-silty, with a relic microbedded structure at the bottom part. The middle part is constituted by a large, red and clayey material, which is disseminated in a grey, silty to clayey silty framework. The mineral assemblage is dominated by quartz, hematite, goethite, kaolinite, with traces

Table 3: Mineralogical composition of the parent rock and the weathered materials at Napene.

Minerals	Minerals										
	Ant.	Mag.	Goeth.	Hem.	Maghe	Talc	Kaol.	Lithio	Gibb	Quartz	Anatase
Loose clayey horizon	-	-	++	++	+	ε	+	-	++	++	+
Pisolitic iron duricrust	-	-	+	+++	++	ε	++	-	ε	+	+
Nodular horizon (nodules)	-	-	++	++	+	ε	+	-	+++	ε	-
Nodular horizon (matrix)	-	-	+	+++	++	ε	++	-	ε	+	-
Fine saprolite (top)	-	-	+	++	-	+	+	+	+	++	-
Fine saprolite (middle)	-	-	++	++	-	ε	++	+	ε	++	-
Fine saprolite (bottom)	-	-	++	++	-	-	+	+	-	++	-
Parent rock	+++	+	-	-	-	-	-	-	-	-	-

Mag.: magnetite; Goeth.: goethite; Hem.: hematite; Kaol.: kaolinite; Lithio.: lithiophorite; Maghe.: maghemite.
+++: very abundant; ++: abundant; +: poorly represented; ε: trace; -: absent.

Table 4: Chemical composition [major elements (in wt %), Pd (in ppb)] of the parent rock and the weathered materials at Napene.

		Parent rock	Fine saprolite			Nodular horizon		Pisolitic iron duricrust	Loose clayey horizon
			base	middle	top	matrix	nodules		
Symbols		NA2	NA8	NA6	NA4	NA1	NA5	NA3	NA7
Depth (m)	-	-	13.70	11.50	10.50	8.50	8.50	5.00	0.50
	D.l.								
SiO_2	0.01	38.99	40.31	38.14	34.78	23.54	7.87	21.19	31.15
Al_2O_3	0.01	1.00	15.91	11.59	13.01	19.51	25.78	20.88	17.70
Fe_2O_3	0.01	7.20	34.91	41.56	40.38	43.04	47.96	42.76	36.72
MnO	0.01	0.16	0.96	0.74	2.00	0.32	0.98	0.17	0.12
MgO	0.01	39.70	< 0.01	0.24	0.69	0.52	0.49	0.11	0.30
CaO	0.01	0.01	< 0.01	0.01	0.01	< 0.01	< 0.01	< 0.01	0.01
Na_2O	0.01	< 0.01	< 0.01	0.02	0.01	0.02	0.01	< 0.01	< 0.01
K_2O	0.01	< 0.01	< 0.01	0.08	0.07	0.05	< 0.01	0.03	0.09
TiO_2	0.01	0.04	0.07	0.21	0.36	0.89	0.36	1.13	1.23
P_2O_5	0.01	< 0.01	0.02	0.03	0.04	0.06	0.03	0.06	0.12
LOI	0.05	12.54	6.92	6.08	7.41	11.06	14.83	11.62	11.91
Sum	-	99.64	99.10	98.70	98.76	99.02	98.31	97.95	99.35
Pd	2.00	< 2	28	26	20	20	19	38	11

Dl.: Detection limit.

of lithiophorite, gibbsite and talc (Table 3, Fig. 8). The geochemical analyses of parent rock (NA2) indicate 38.99 wt.% SiO_2, 39.70 wt.% MgO, 7.20 wt.% Fe_2O_3,, 1.00 wt.% Al_2O_3. At the bottom, SiO_2 increases from 38.99 wt.% to 40.31 wt.%. Fe_2O_3 contents rise from 7.20 wt.% to 34.91 wt.%, like those of Al_2O_3 contents (1.00 wt.% to 15.91 wt.%). MgO decreases from 39.70 wt.% to 0.96 wt.%. In the middle part, SiO_2 and Al_2O_3 contents decrease (38.14% SiO_2, 11.59% Al_2O_3) whereas those of Fe_2O_3 increase (41.56%). Accessorily, the fine saprolite is composed of 0.24% MgO, 0.21% TiO_2, 0.74% MnO and 0.03% P_2O_5 (Table 4). At the top, it is constituted by a greyish red material. The mineral assemblage is dominated by quartz, hematite and small amounts of goethite, talc, kaolinite, lithiophorite and gibbsite (Table 3). The geochemical analyses indicate a decrease in SiO_2 and Fe_2O_3 contents (34.78% SiO_2 and 40.38% Fe_2O_3), and an increase in Al_2O_3 (13.01%) and MnO (2.00%) contents. Accessorily, it is composed of 0.69% MgO, 0.36% TiO_2, 0.74% MnO and 0.04% P_2O_5 (Table 4).

The fine saprolite transforms to the nodular horizon (3 m). It is constituted by a matrix which binds the nodules together. This matrix is yellowish brown and slightly hardened and is composed of hematite, maghemite, kaolinite, quartz, goethite, and small amounts of gibbsite and talc (Table 3). SiO_2 contents decrease to 23.54%, while those of Al_2O_3 and Fe_2O_3 increase (19.51% Al_2O_3 and 43.04% Fe_2O_3). Accessorily, it is composed of 0.52% MgO, 0.89% TiO_2, 0.32% MnO and 0.06% P_2O_5 (Table 4).

Table 5: Mineralogical composition of the parent rock and the weathered materials at Mang North.

Materials	Minerals					
	Antigorite	Quartz	Magnetite	Hematite	Goethite	Kaolinite
Loose clayey horizon	-	+	-	+++	-	+
Nodular horizon (pisolitic iron duricrust)	-	+	-	++	++	+
Nodular horizon (matrix)	-	+	+	-	+++	+
Nodular horizon (bottom)	-	+	+	-	+++	+
Fine saprolite	-	+	+	-	+++	+
Coarse saprolite	-	+	+	-	+++	+
Parent rock	+++	-	++	-	-	-

+++: very abundant; ++: abundant; +: poorly represented; ε: trace ; -: absent.

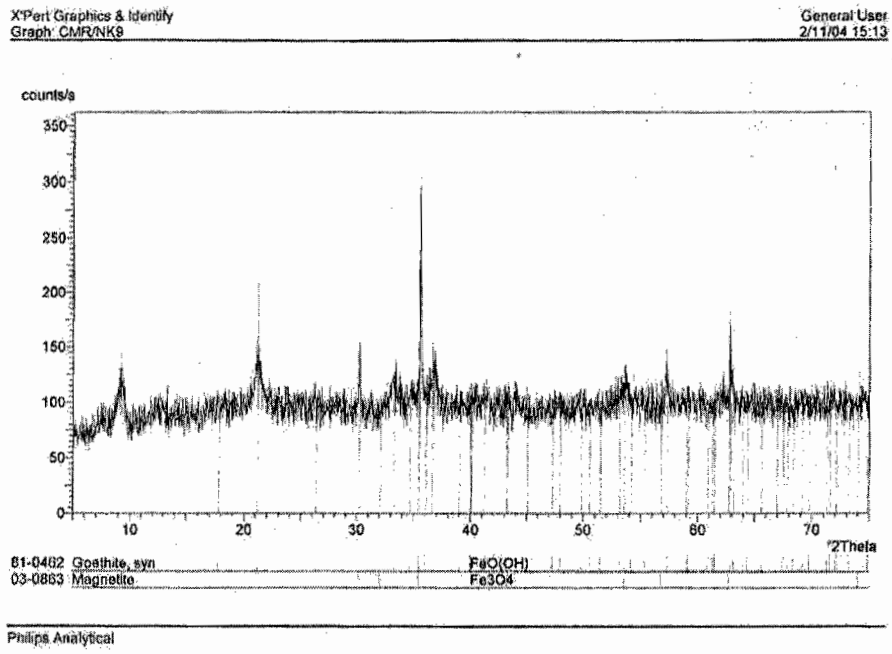

Figure 5: X-ray diffraction spectrum of the coarse saprolite.

The nodules are either flattened or rounded, reddish brown and slightly hardened. The difference between the matrix and the nodules is based on the amounts of gibbsite, kaolinite, maghemite and quartz (Table 3, Fig. 9). SiO_2 contents decrease considerably (7.87%), whereas those of Al_2O_3 and Fe_2O_3 instead increase highly (25.78% Al_2O_3 and 47.96% Fe_2O_3). Accessorily, the nodules are composed of 0.69% MgO, 0.36% TiO_2, 0.74% MnO and 0.04% P_2O_5 (Table 4). The nodular horizon is overlained by the pisolitic iron duricrust.

The pisolitic iron duricrust (4.5 m) is constituted by metric blocks held together by a ferruginous matrix. The matrix is much less abundant (~10 %), loose and reddish. The pisolites are either spherical or flattened, reddish brown and

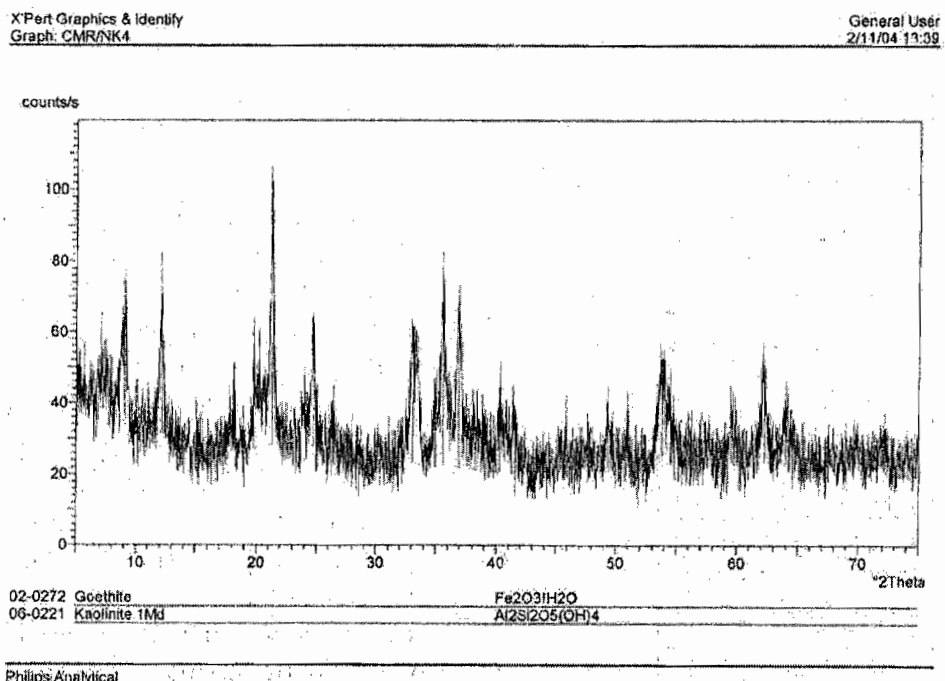

Figure 6: X-ray diffraction spectrum of nodules (Upper nodular horizon).

connected by hardened matrix. The pisolitic iron duricrust contains hematite, maghemite, kaolinite, quartz and small amounts of goethite, anatase, talc and gibbsite (Table 3). The geochemical analyses indicate an increase in SiO_2 contents from the nodules to the pisolitic iron duricrust (7.87 to 21.19 %) and a decrease in Al_2O_3 and Fe_2O_3 contents (25.78 to 20.88% Al_2O_3, 47.96 to 42.76 % Fe_2O_3, in Table 4). Accessorily, the pisolitic iron duricrust is composed of 0.11% MgO, 1.13% TiO_2, 0.17% MnO and 0.06% P_2O_5 (Table 4).

The pisolitic iron duricrust dismantles to the loose clayey horizon (2.5 m). This loose clayey layer is dark red, and polyhedral at the bottom to slightly lumpy at the sub-surface. The mineral assemblage is dominated by hematite, goethite, gibbsite, quartz, and small amounts of maghemite, kaolinite, anatase and talc (Table 3, Fig. 10). SiO_2 contents increase (31.15%), while those of Al_2O_3 and Fe_2O_3 instead decrease (respectively 17.70 wt% and 36.72 wt.%).

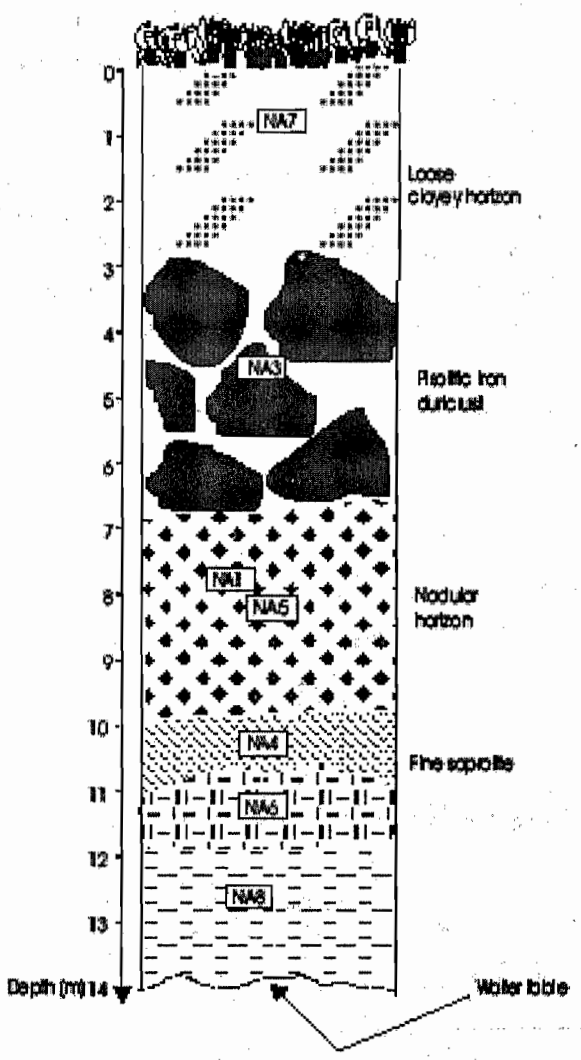

Figure 7: Description of Napene weathering profile.

4.2.3. Mang North weathering profile

The weathering profile is situated at the centre of the Mang North ultramafic body (Fig. 3). It is 18.70 m thick above the water table and can be divided, from bottom to top, into four main layers: coarse saprolite, fine saprolite, nodular horizon and loose clayey horizon (Fig. 11).

The coarse saprolite (5.70 m) is dark brownish red, sandy-silty to silty-clayey, polyhedral and loose. The framework has three types of centimetric patches: microbedded patches, greenish yellow patches and dark patches. The mineralogical analyses indicate the presence of goethite, kaolinite and quartz, and magnetite traces (Table 5). The geochemical analyses of parent serpentinite (MA6) indicate 37.33 wt.% SiO_2, 38.20 wt.% MgO, 7.34 wt.% Fe_2O_3 and 2.27 wt.% Al_2O_3 (Table 6). From the parent rock to the coarse saprolite, Fe_2O_3 and Al_2O_3 contents increase (67.22 wt.% Fe_2O_3 and 9.55 wt.% Al_2O_3), whereas those of SiO_2 and MgO instead strongly decrease (9.49 wt.% SiO_2, 0.33 wt.% MgO, in Table 6). MnO contents increase from 0.08 to 1.17 wt.%.

The coarse saprolite progressively transforms to the fine saprolite (4 m). This horizon is loose, reddish brown, polyhedral, clayey to sandy. It contains patches showing a microbedded structure and abundant centimetric dark patches. The mineral assemblage is the same as that of the coarse saprolite (Table 5), in spite of a different organization of the materials. A SEM micrograph of a section of the fine saprolite confirms the presence of quartz (Fig. 12). The origin of quartz is unclear. It may result from the downward transport of surficial material along fractures induced by skrinkage during weathering or leaching, it may have formed in situ from silica-rich solutions. In the chemical point of view, a minor decrease in Fe_2O_3 contents and a minor

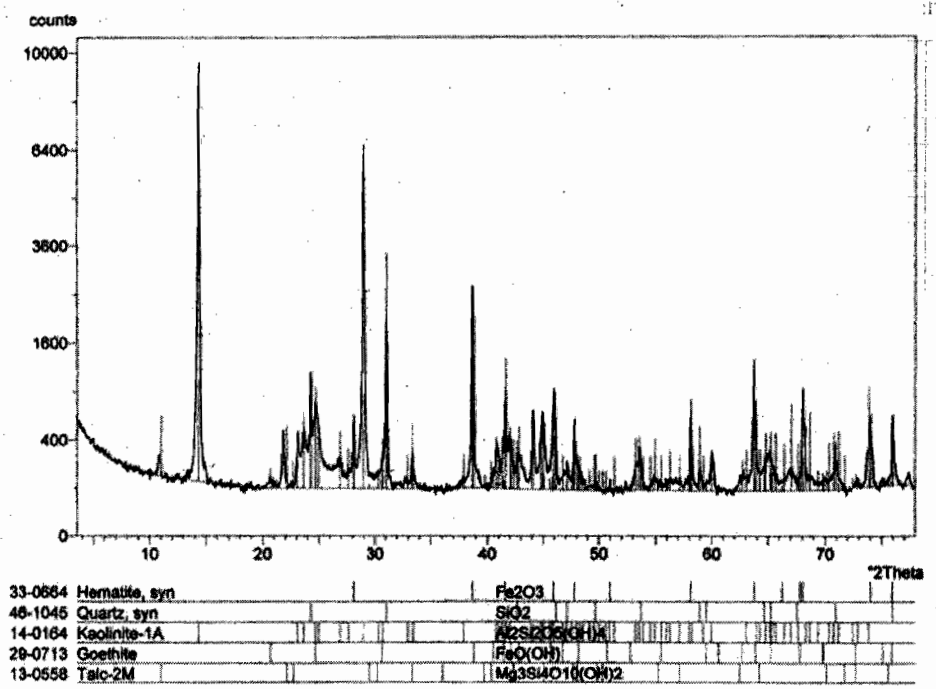

Figure 8: X-ray diffraction spectrum of the fine saprolite.

increase in SiO_2 and Al_2O_3 contents are observed (Table 6). At the top, the fine saprolite alters to the nodular material.

The nodular horizon (8 m) is made up of nodules and blocks of iron duricrust, embedded in a matrix. The bulk sample of the bottom is mainly goethitic and hematitic, in spite of the presence of small amounts of magnetite, kaolinite and quartz (Table 5). The decrease in Fe_2O_3 contents continues, accompanied by a similar drop in SiO_2 and a rise in Al_2O_3 contents (Table 6). Accessorily, the horizon is composed of 0.23% MgO, 0.81% TiO_2, 0.17% MnO and 0.05% P_2O5 (Table 6).

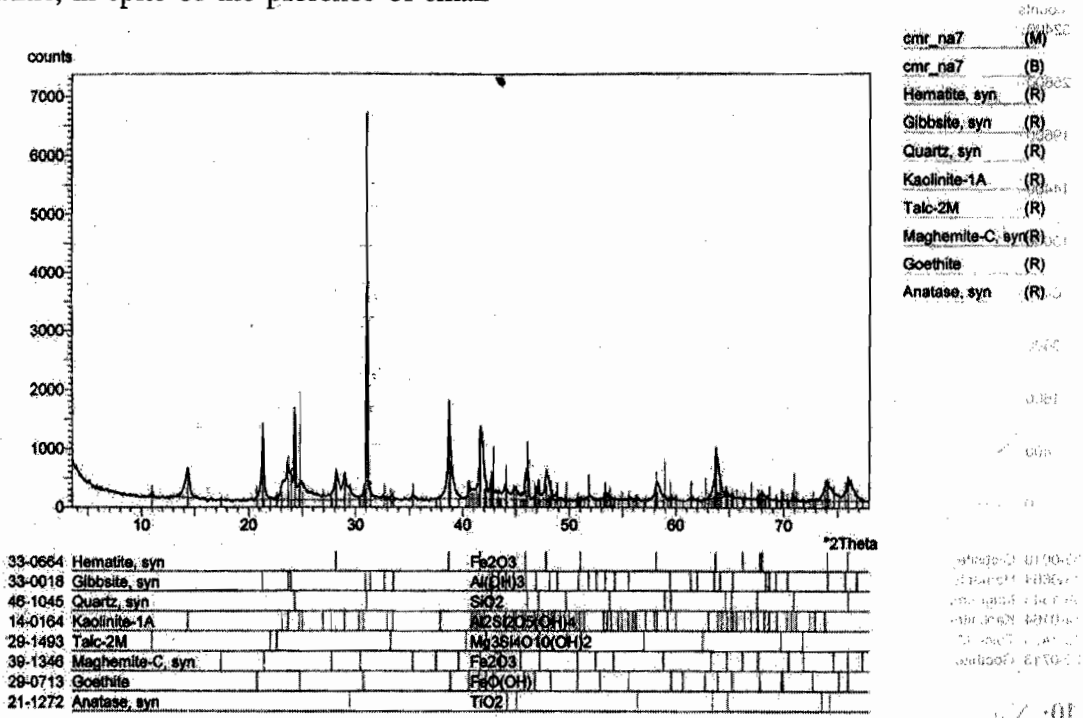

Figure 9: X-ray diffraction spectrum of nodules (Nodular horizon).

Table 6: Chemical composition [major elements (in wt %), Pd (in ppb)] of the parent rock and the weathered materials at Mang North body.

		Parent rock	Coarse saprolite	Fine saprolite	Nodular horizon			Loose clayey horizon
					base	matrix	nodules	
Symbols		MA6	MA5	MA2	MA7	MA1	MA3	MA4
Depth(m)	-	-	15.00	10.50	8.50	4.50	4.50	0.50
	D.I.							
SiO_2	0.01	37.33	9.49	12.86	10.48	12.48	14.33	16.22
Al_2O_3	0.01	2.27	9.55	12.03	18.68	19.48	26.18	22.87
Fe_2O_3	0.01	7.34	67.22	62.71	53.40	47.10	39.24	44.63
MnO	0.01	0.08	1.17	1.20	1.07	0.19	0.07	0.18
MgO	0.01	38.2	0.33	0.29	0.23	0.12	0.06	0.22
CaO	0.01	0.61	< 0.01	< 0.01	< 0.01	< 0.01	< 0.01	< 0.01
Na_2O	0.01	0.03	0.02	< 0.01	< 0.01	0.01	< 0.01	< 0.01
K_2O	0.01	< 0.01	< 0.01	< 0.01	0.02	0.02	< 0.01	0.05
TiO_2	0.01	0.02	0.15	0.22	0.81	1.74	1.81	1.61
P_2O_5	0.01	< 0.01	< 0.01	< 0.01	0.05	0.01	0.06	0.12
LOI	0.05	13.11	9.36	8.87	12.2	14.19	15.69	13.55
Sum	-	98.99	97.29	98.18	96.94	95.34	97.44	99.45
Pd	0.11	0.27	40	28	17	18	33	14

D.I.: Detection limit.

The matrix (~20 % of the soil) is loose, purplish to yellowish brown, and polyhedral. The mineral assemblage is dominated by goethite and kaolinite, alongside magnetite and quartz traces (Table 5). The geochemical analyses indicate a minor increase in SiO_2 and Al_2O_3 contents (19.48 wt.% SiO_2 and 19.48 wt.% Al_2O_3) and a progressive decrease in Fe_2O_3 contents (47.10 wt.%, in Table 6). Accessorily, the horizon is composed of 0.12% MgO, 1.74% TiO_2, 0.19% MnO and 0.01% P_2O_5 (Table 6).

The iron duricrust blocks are very abundant (~65 % of total volume) and mainly pisolitic. These blocks are made up of a yellowish brown ferruginous cement that coats the pisolites. The mineral assemblage is dominated by goethite, hematite, kaolinite and quartz (Table 5). The geochemical analyses indicate an increase in SiO_2 and Al_2O_3 contents and a decrease in Fe_2O_3

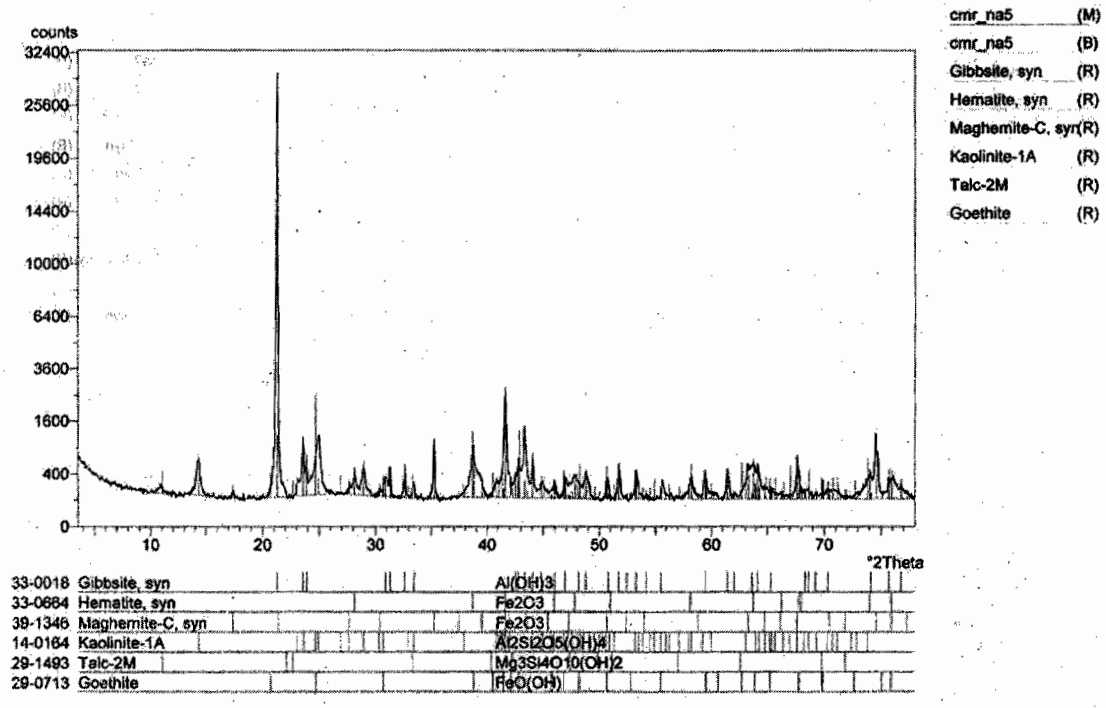

Figure 10: X-ray diffraction spectrum of the loose clayey horizon.

contents relative to the matrix (Table 6). The nodular material dismantles to clayey surface soil. The loose clayey horizon (1 m) is a reddish material and has a polyhedral to crumbly structure. The mineralogical characterization indicates the presence of hematite, kaolinite and quartz (Table 5). The geochemical analyses indicate a slight increase in SiO_2 and Fe_2O_3 contents (16.22 wt.% SiO_2, 44.63 wt.% Fe_2O_3), and a minor decrease in Al_2O_3 contents (Table 6). Accessorily, the loose clayey horizon is composed of 0.22% MgO, 1.61% TiO_2, 0.18% MnO and 0.12% P_2O_5 (Table 6).

4.2.4. Comparison of the three weathering profiles

The Nkamouna and the Mang North profiles contain relic structures of the parent rock. The three profiles show thick hardened ferruginous materials (~8 m). Two profiles (Nkamouna and Mang North) are characterized by high Fe_2O_3 contents in the saprolite. Meanwhile, the Napene profile is rather more enriched in SiO_2 than the others. Al_2O_3 contents increase along the three profiles as TiO_2.

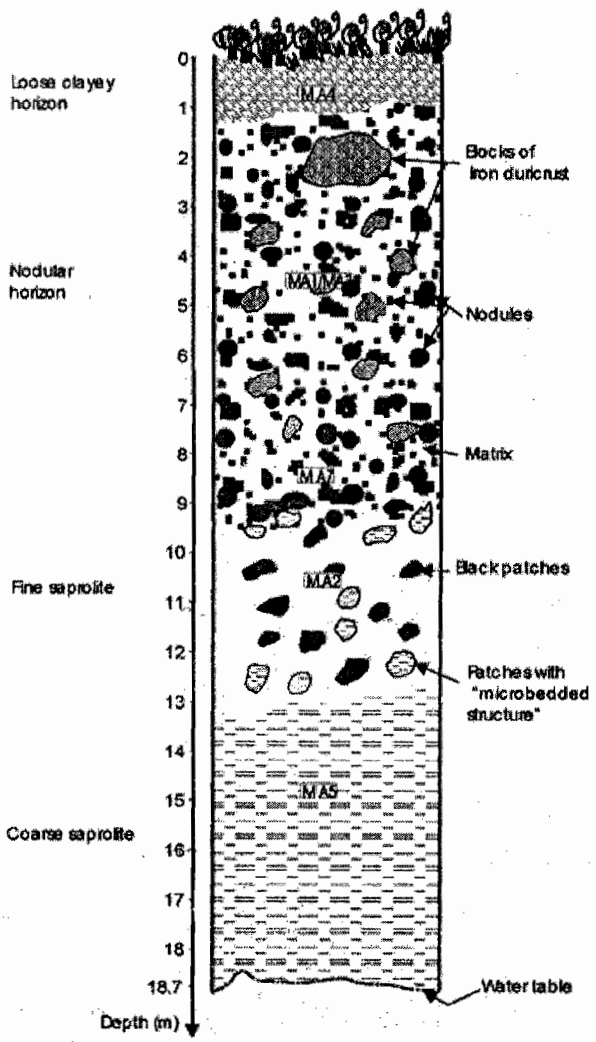

Figure 11: Description of Mang North weathering profile.

4.3. Palladium behaviour in the weathered materials

4.3.1. Distribution of palladium in the weathering profiles

The Pd contents vary between 10 and 22 ppb in the Nkamouna profile (Table 2). Palladium reaches 15 ppb at the bottom of the coarse saprolite and 12 ppb in the uppermost part of the same saprolite, and 13 ppb in the fine saprolite. In the lower nodular horizon, Pd contents remain close to 13 ppb in the matrix and 20 ppb in the brown nodules. In the upper nodular horizon, the Pd contents are 11 ppb in the matrix and attain their maximum value (22 ppb) in the multilobed nodules (Table 2). This Pd contents decrease sharply in the clayey surface soil (10 ppb).

At Napene site, the Pd contents are slightly higher than those observed in the Nkamouna materials. Pd values oscillate between 11 and 38 ppb (Table 4). In the fine saprolite, Pd contents are 28 ppb at the bottom of saprolite, 26 ppb at the middle part of the same horizon and 20 ppb at the top. In the nodular horizon, the Pd contents also remain close to 20 ppb in the matrix and decrease to 19 ppb in the nodules. Palladium contents attain the maximum value in the pisolitic iron duricrust (38 ppb), and then reduce to 11 ppb in the clayey surface soil (Table 4).

At Mang North site, Pd contents are higher than in the last two profiles. They oscillate between 17 and 40 ppb (Table 6). Palladium contents are at a maximum in the coarse saprolite (40 ppb) and decrease to 28 ppb in the fine saprolite. In the bulk fraction of the nodular horizon, the palladium contents are 17 ppb and increase slightly in the matrix at the upper part (18 ppb), and practically double in the pisolitic iron duricrust (33 ppb). In the clayey surface soil, palladium contents are 13 ppb (Table 6).

Palladium contents are high in the coarse saprolite (Mang North profile), in the nodules (Nkamouna profile) and the pisolitic iron duricrust (Napene profile). Apart from the coarse saprolite from the Mang North profile, palladium contents are lower in the loose materials than in the hardened materials. The palladium values decrease from the saprolite zone upwards into the clayey surface soil, except in hardened materials.

4.3.2. Palladium behaviour versus Fe, Si, Al

In the tropical zone, supergene weathering provokes the leaching of all elements (Ndjigui et al. 2008). The elements which remain in this weathering environment are Fe, Si and Al (Tardy 1993). Among these elements, Fe is the most abundant in the laterites mostly developed on ultramafic rocks (Eno Belinga 1983; Tardy 1993; Traoré et al. 2006; Yongué-Fouateu et al. 2006). Binary diagrams were established using the concentrations of four elements (Fe, Si, Al and Pd) (Fig. 13); they reveal that:

- at Nkamouna site, Fe_2O_3 shows a negative correlation with Pd (Fig. 13a), while correlation between SiO_2/Pd (Fig. 13b) and Al_2O_3/Pd (Fig. 13c) is positive;
- at Napene site, correlations between the three most abundant major elements and Pd are not clearly defined (Fig. 13d-f). SiO_2/Pd and Al_2O_3/Pd show a relatively positive correlation (Fig. 13e-f);
- at Mang North site, Fe_2O_3 has a positive correlation with Pd (Fig. 13g), meanwhile SiO_2 and Al_2O_3 show a negative correlation with Pd (Fig. 13h-i).

Pd behaviour versus the three most abundant major elements (Fe, Si, Al) is not uniform in the weathering profiles of the Lomié ultramafic complex.

5. DISCUSSION

The high Pd contents in the coarse saprolite result either from the supergene enrichment or secondary

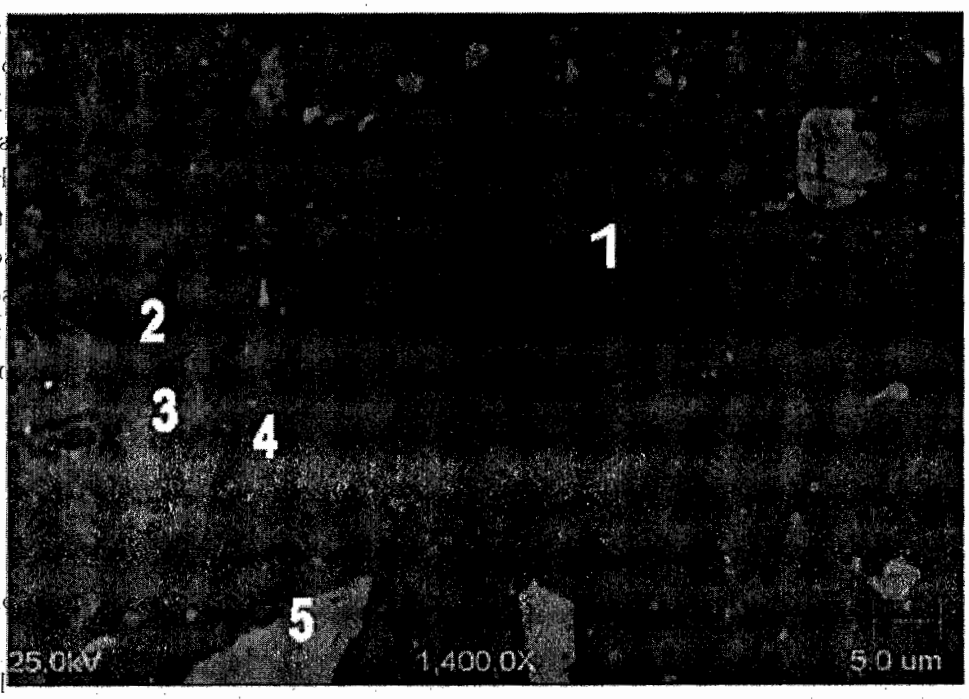

Figure 12a: Back-scattered electron image of the fine saprolite (Mang North site).
It is a part of the fine saprolite which is more weathered. We note the presence of Fe-oxides rich in Cr (plot 1); relic zone which contains Mg, Si and Fe-oxides (plot 2); Mn-oxides rich in Fe, Al, Ni and Co (plot 3); Fe-oxides rich in Al, Mn and Ni (plot 4); relic or formed in situ grain of quartz? (plot 5). The black patches represent the voids network.

Pd precipitation processes (Salpéteur et al. 1995; Wood and Middlesworth 2004). Wood and Normand (2008) have shown that palladium is mobilized as a chloride complex which can be easily transported with oxidizing-buffering capacity. This process can also explain the supergene enrichment of palladium in the saprolite. The coarse saprolite possesses the most favourable oxidizing conditions of PGE supergene enrichment, like palladium (Azaroual et al. 2001).

The low Pd contents observed in the loose materials as well as the progressive decrease of palladium contents from the saprolite zone to the clayey surface soil could be attributed to an intense leaching (Augé et al. 1995; Salpéteur et al. 1995; N[illegible]ui et al. 2004) or chemical dispersion (Evans et al. 1994). The low Pd contents could be due to its higher mobility relative to the other PGE (Prichard and Lord 1994). These processes might be facilitated by the infiltration of water charged with organic ligands (acetate and oxalate) and CO_2

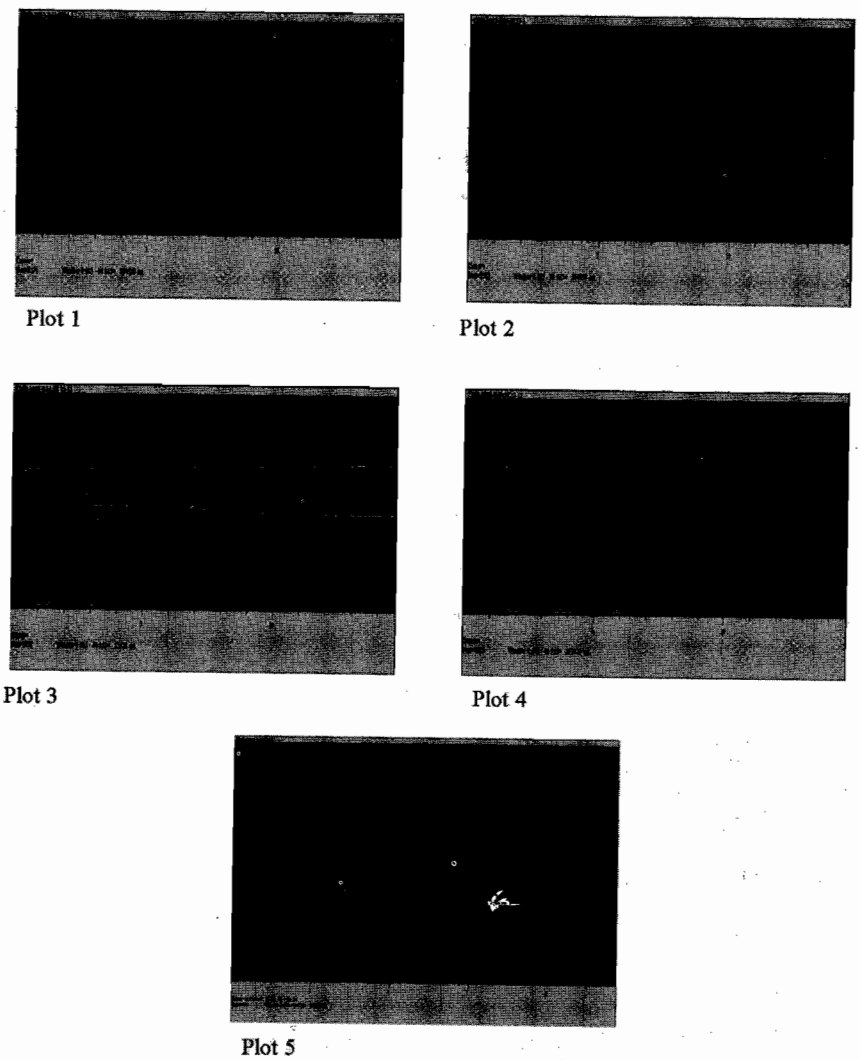

Figure 12b: Chemical microanalyses in fine saprolite (plots 1-5).

percolating through the weathering profiles (Wood 1996; Wood and Middlesworth 2004).

In the hardened materials, the high Pd contents could be favoured by the extremely hardened nature of the iron. Varajao et al. (2000) attributed the high Pd contents of the ferricretes, at the Maquiné Mine area (Brazil), to the highly hardened nature of the iron, which also favours quartz and hematite stability.

Salpéteur et al. (1995) showed that Pd behaviour is similar to that of Si in the Madagascar laterites. This hypothesis is verified in the Nkamouna and Napene weathering materials. Singh et al. (2002) document that several metals like Ni, Cr, Pd, Pt are in the structures of Fe-oxides, the negative correlation between Si and Pd, Aluminium and palladium confirms that kaolinite or quartz can not fixed some metals in their structures. The negative correlation between Fe_2O_3 and Pd in the Nkamouna weathering materials shows that supergene weathering concentrates Fe at the bottom of profiles and sometimes palladium in the nodules of the upper horizons. At Mang North, Fe_2O_3 has a positive correlation with Pd. Traoré et al. (2006) have shown that Fe and Pd can be depleted by eluviation processes. The dissolution of palladium and Fe-oxides in the upper part of profiles by organic ligands (acetate and oxalate) could be at the origin of palladium supergene enrichment in the coarse saprolite (Wood 1996).

6. CONCLUSIONS

1. The Pd behaviour in the three lateritic profiles is complex. The elevated Pd contents in coarse saprolite are due to the supergene enrichment and secondary Pd precipitation processes.
2. The elevated Pd contents in nodules and pisolitic iron duricrust are attributed to the indurated nature of the iron.

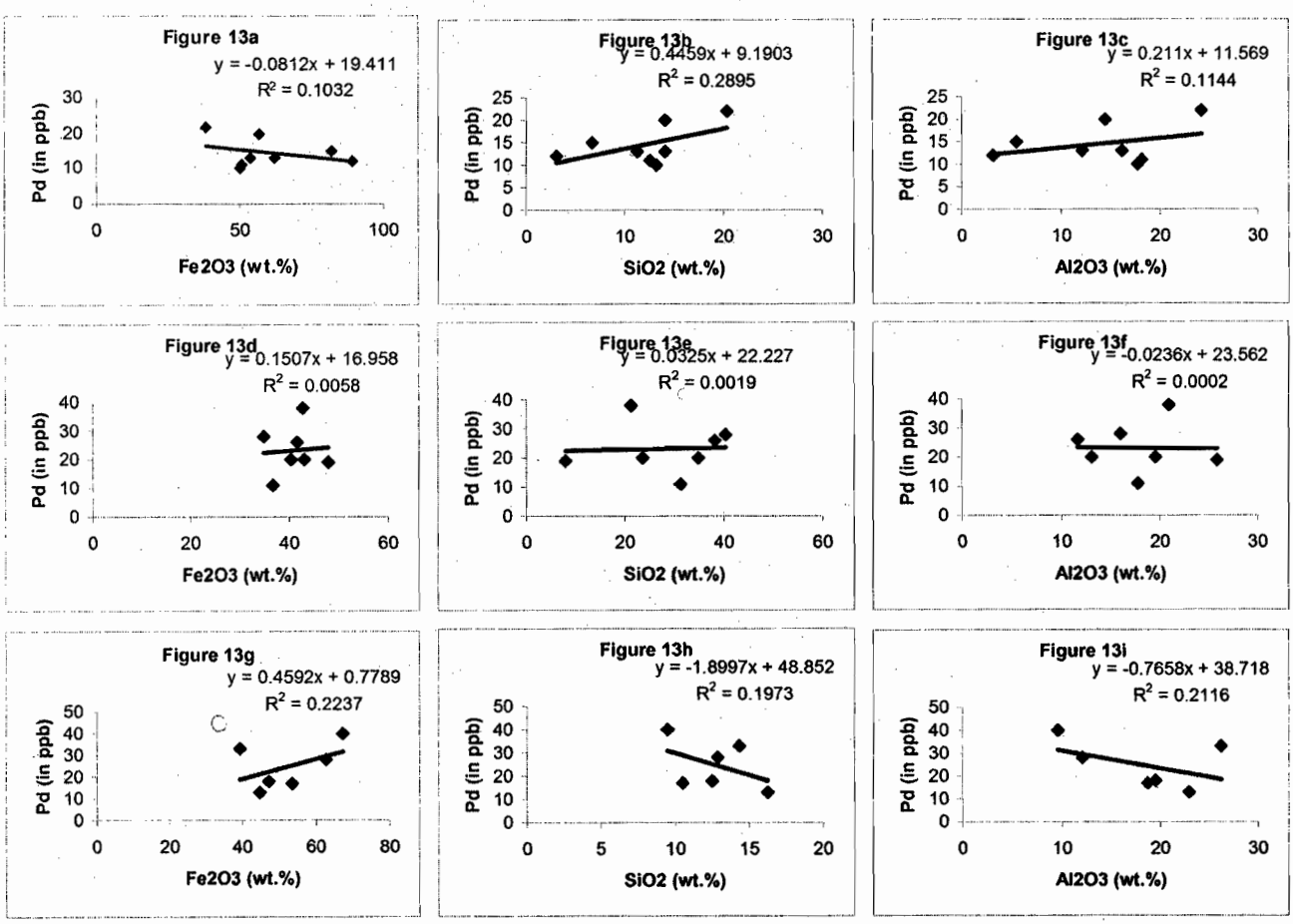

Figure 13 : Binary variation in Fe_2O_3 vs Pd, SiO_2 vs Pd, Al_2O_3 vs Pd diagrams for the ultramafic weathering materials: Nkamouna site (13a-c); Napene site (13d-f) and Mang North site (13g-i).

3. Fe_2O_3 versus Pd binary diagrams show a negative correlation in the Nkamouna weathered materials and a positive one in those of Mang North. The SiO_2 versus Pd and Al_2O_3 versus Pd binary diagrams present a positive correlation in the Nkamouna and Napene weathered materials, and negative one in the Mang North profile.

ACKNOWLEDGEMENTS

This work is partially supported by grants from the Geology Department of the University of Toronto (Canada) for stages of samples preparation and analysis, the author is grateful to Professor James E. Mungall. I am grateful to Professors Ekodeck Georges Emmanuel and C. Emmanuel Suh for their insightful reviews that significantly improved the quality of this paper. I thank professors James E. Mungall and Hazel M. Prichard (University of Cardiff, UK) for their help and fruitful discussions. This work is a contribution to IGCP 479 Project.

REFERENCES

Auget T., Maurizot P., Breton J., Eberle JM., Gilles C., Jezequel P., Meziere J., Robert M., (1995) Magmatic and supergene platinum-group minerals in the New Caledonia ophiolite. Chron. rech. min. 520, pp. 3-36.

Azaroual M., Romand B., Freyssinet P., Disnar J., (2001) Solubility of platinum in aqueous solutions at 25°C and pHs 4 to 10 under oxiding conditions. Geochim. Cosmochim. Acta 65 (24), pp. 4453-4466.

Bowles J.F.W., (1986) The development of platinum-group minerals in laterites. Economic Geology 81, pp. 1278-1285.

Eno Belinga S.M., (1983) Géologie dynamique externe des pays tropicaux de la Terre: Afrique, Amérique, Asie. Les paysages du fer. Librairie universitaire de Yaoundé, 306 p.

Evans D.M., Buchanan D.L., Hall G.E.M., (1994) Dispersion of platinum, palladium and gold from the Main Sulphide Zone, Great Dyke, Zimbabwe. Transactions of the Institution of Mining and Metallurgy 103, B57-B67. (Section B: Applied earth science).

Godel B., Barnes S.-J., (2007) Platinum-group elements in sulphide minerals and the whole rocks of the J-M Reef (Stillwater complex): Implication for the formation of the reef. Chemical Geology, doi:1016/ j.chemgeo.2007.05.2006.

Godel B., Barnes S.-J., Maier W.D., (2007) Platinum-group elements in sulphide minerals, platinum-group minerals, and whole rocks of the Merensky Reef (Bushveld complex, South Africa): Implications for the formation of the reef. Journal of Petrology 48, 8, pp. 1569-1604.

Lasserre M., Soba D., (1976) Age libérien des granitoïdes et des gneiss à pyroxènes du Cameroun méridional. Bull. BRGM 2, VI (1), pp. 17-32.

Letouzey R., (1985) Notice explicative de la carte phytogéographique du Cameroun à l'échelle de 1/500 000. Institut de la Carte Internationale de Végétation, Toulouse, 240 p.

Luguet A., Shorey S.B., Lorand J.P., Horan M.F., Carlson R.W., (2007) Residual platinum-group minerals from highly depleted harzburgites of the Lherz massif (France) and their role in HSE fractionation of the mantle. Geochimica et Cosmochimica Acta 71, pp. 3082-3097.

Ndjigui P.-D., Bilong P., Bitom D., Dia A., (2008) Mobilization and redistribution of major and trace elements in two weathering profiles developed on serpentinites in the Lomié ultramafic complex, South-East Cameroon. Journal of African Earth Sciences, 50, pp. 305-325.

Ndjigui P.D., Bitom D., Bilong P., Colin F., Hendratta N.A., (2003) Influence des oxydes métalliques (Fe2O3, Cr2O3, NiO) sur le comportement du platine et du palladium dans les manteaux d'altération des roches ultrabasiques serpentinisées en zone forestière humide d'Afrique Centrale. Annales de la Faculté des Sciences, Univ. de Yaoundé I, Sér. Sciences de la Terre et Sciences de la Vie 35 (2), pp. 4-13.

Ndjigui P.D., Mungall J.E., Bilong P., (2004) Behaviour of PGE in the Mang North weathering profile on serpentinite in the Lomié ultrabasic complex (South-East Cameroon). Proceedings of Recent Advances in Magmatic Ore Systems of Mafic-Ultramafic Rocks, IGCP 479 Hong Kong, pp. 129-134.

Prichard M.H., Lord R.A. (19940 Evidence for the secondary environment in Shetland ophiolite complex. Transactions of the Institution of Mining and Metallurgy 103, B57-B67. (Section B: Applied earth science).

Richardson T., Burnham O.M., (2002) Precious metal analysis at the Geoscience Laboratories: results from the new low-level analytical facility. In Summary of Field Work and Other Activities 2002, Ontario Geological Survey, Open File Report 6100, 35, pp. 1-5.

Salpeteur I., Martel-Jantin B., Rakotomanana D., (1995) Pt and Pd mobility in ferralitic soils of the West Andriamena area (Madagascar). Evidence of a supergene origin of some Pt and Pd minerals. Chron. rech. min. 520, pp. 27-45.

Seme Mouangue A.C., (1998) Géochimie, métamorphisme et métallogénie des formations du secteur

est de Lomié. Th. Doc. 3e cycle, Univ. de Yaoundé I, 155 p.

Singh B., Sherman D.M., Wells M.A., Mosselmans J.F.W., (2002) Incorporation of Cr, Mn and Ni into goethite (α -FeOOH): mechanism from extended X-ray absorption fine structure spectroscopy. Clay Miner. 37 pp. 639-649.

Suchel J.-B., (1987) Les climats du Cameroun. Thèse, université de Bordeaux III, 1186 p.

Tardy Y., (1993) Pétrologie des latérites et des sols tropicaux. Ed Masson, Paris, 459 p.

Toteu S.F., Yongue-Fouateu R., Penaye J., Tchakounte J., Seme Mouangue A.C., Van Schmus W.R., Deloule E., Stendal H., (2006) U-Pb dating of plutonic rocks involved in the nappe tectonic in southern Cameroon: consequence for the Pan-African orogenic evolution of the central African fold belt. Journal of African Earth Sciences 44, pp. 479-493.

Traore D., (2005) Serpentinisation hydrothermale et altération latéritique des roches ultrabasiques en milieu tropical : évolution minéralogique et géochimique de la minéralisation en platine de la Rivière des Pirogues, Nouvelle-Calédonie. PhD thesis, Université de la Nouvelle-Calédonie, 193 p.

Traore D., Beauvais A., Auge E T., Chabaux F., Parisot J.-C., Cathelineau M., Peiffert C., Colin F., (2006) Platinum and palladium mobility in supergene environment: the residual origin of the Pirogues River mineralization, New Caledonia. Journal of Geochemical Exploration 88, pp. 350-354.

Varajao C.A.C., Colin F., Viellard P., Melfi A.J., Nahon D., (2000) Early weathering of palladium gold under lateritic conditions, Maquiné Mine, Minas Gerais, Brazil. Applied Geochemistry 15, pp. 245-263.

Wood S.A. (1996) The role of humic substances in the transport and fixation of metals of economic interest (Au, Pt, Pd, U, V). Ore Geology Reviews 11, pp. 1-31.

Wood S.A., Middlesworth J.V., (2004) The influence of acetate and oxalate as simple organic ligands on the behaviour of palladium in surface environments. The Canadian Mineralogist 42, pp. 411-421.

Wood S.A., Normand C., (2008) Mobility of palladium chloride complexes in mafic rocks: insights from a flow-through experiment at 25°C using air-saturated, acid, and Cl-rich solutions. Journal of Petrology, 92 (1), pp. 81-97.

Yongue-Fouateu R., (1995) Les concentrations métallifères de nickel et de cobalt à partir de l'altération latéritique des roches ultrabasiques serpentinisées du Sud-Est Cameroun. Thèse, Université de Yaoundé 1, 262 p.

Yongue-Fouateu R., Ghogomu R.T., Penaye J., Ekodeck G.E., Stendal H., Colin F., (2006) Nickel and cobalt distribution in the laterites of the Lomié region, south-east Cameroon. Journal of African Earth Sciences 45, pp. 33-47.

Received: 28/05/07

Accepted: 04/03/08